Probabilistic Control Optimization of Aeroservoelastic Systems with Uncertainty

Liam J. Adamson *, Sebastiano Fichera † and John E. Mottershead ‡
University of Liverpool, Liverpool, L69 3GH, United Kingdom

A probabilistic-based control optimization method is developed for aeroservoelastic systems with parameter uncertainties. Genetic algorithms are used to find optimal feedback control gains that simultaneously assign a mean flutter speed and maximize a defined worst-case speed. In the proposed approach, a surrogate model of the flutter speed response surface is constructed so that the critical flutter speed is represented in terms of the uncertain parameters. The surrogate model is created in two ways: 1) by linearization of the response surface using local sensitivities, and 2) by a polynomial chaos expansion. The surrogate model is then sampled to find the worst-case flutter speed, which is defined probabilistically by the inverse cumulative distribution function. The method is applied to a three-degree-of-freedom aeroservoelastic system that uses an unsteady, two-dimensional potential flow and explicitly contains the control and actuator dynamics. Case studies with uncertainty in the pitch and plunge stiffness parameters are presented. It is demonstrated that the control gains have a strong influence on the shape of the response surface and that it is possible to control not only the expectation, but also the variance of the flutter speed.

I. Nomenclature

$\mathbf{A}$	=	state matrix
a_i	=	polynomial chaos expansion coefficients
$\mathbf{C}_a$	=	aerodynamic-equivalent damping matrix
$\mathbf{C}_c$	=	control-equivalent damping matrix
$\mathbf{C}_s$	=	structural damping matrix
$\mathbf{f}$	=	velocity feedback gain vector
$\mathbf{f}_a$	=	aerodynamic force vector
$\mathbf{f}_c$	=	control force vector
F^{-1}	=	inverse cumulative distribution function
$\mathbf{g}$	=	position feedback gain vector
h	=	plunge displacement
$\mathbf{K}_a$	=	aerodynamic-equivalent stiffness matrix
$\mathbf{K}_c$	=	control-equivalent stiffness matrix
$\mathbf{K}_s$	=	structural stiffness matrix
k_d	=	derivative gain of PID
k_h	=	plunge stiffness
k_i	=	integral gain of PID
k_p	=	proportional gain of PID
k_t	=	torque constant
k_α	=	pitch stiffness
L	=	aerodynamic lift
$\mathbf{M}_a$	=	aerodynamic-equivalent mass matrix
$\mathbf{M}_c$	=	control-equivalent mass matrix
$\mathbf{M}_s$	=	structural mass matrix
M_α	=	aerodynamic moment about the pitch

*PhD Researcher, Department of Mechanical, Materials and Aerospace Engineering.
†Lecturer in Aerospace Engineering, Department of Mechanical, Materials and Aerospace Engineering, AIAA Member.
‡Professor of Applied Mechanics, Department of Mechanical, Materials and Aerospace Engineering, AIAA Member.

M_β = aerodynamic moment about the control surface
$\mathbf{N}_c$ = integral matrix
$\mathbf{q}$ = vector of degrees-of-freedom
T_β = control torque
u = control current
v = freestream speed
$\mathbf{x}$ = state vector
α = pitch angle
β = control surface deflection
β_d = desired control surface deflection
ζ = random parameter
$\boldsymbol{\phi}$ = aerodynamic state vector
$\boldsymbol{\phi}_{L,R}$ = left and right eigenvectors of the state matrix
Ψ = orthogonal function

II. Introduction

The use of active control to suppress aeroelastic flutter is a now well-established technique that has been applied successfully numerically and in a multitude of experimental systems [1]. With a suitable choice of control law, it is possible to favorably modify aeroelastic modes in terms of frequency and damping such that either: 1) the flutter speed is increased, or 2) the flutter mechanism is mitigated entirely [2]. Usually, active control requires accurate modelling of the system under study. This is difficult in aeroservoelastic systems, however, since there often exists uncertainty in the structural and aerodynamic parameters [3]. Such uncertainties may arise from variable operating conditions, structural or material degradation, and manufacturing variability. As a consequence, aeroservoelastic systems may exhibit uncertain flutter boundaries [4].

Typically, the abovementioned problem is addressed using robust control techniques such as μ-synthesis [5]. In these approaches, uncertain parameters are modelled as bounded sets and are represented by a linear fractional transformation to a nominal system. A controller is then chosen so that the system is guaranteed to be stable within the ranges of the uncertain parameters. Literature in this field is extensive and a detailed survey may be found in the review by Yuting and Chao [6]. Although such techniques are simple to implement, they can lead to overly-conservative controllers if the chosen parameter bounds are not selected well [7, 8].

In recent years, it has been proposed that uncertainty quantification (UQ) techniques should be applied to aeroelastic systems [9–11]. The advantage of UQ is that probabilistic information from the sources of uncertainty can be exploited to predict the likelihood of flutter or other aeroelastic phenomena. In this way, servo-structural systems may be optimized subject to reliability based-constraints and without the need to define arbitrary parameters bounds [12]. A probabilistic-based optimization was considered by Manan and Cooper [13], who used a particle swarm approach to optimize the layup orientation of a composite wing with an uncertain laminae thickness and Young's modulus. The probability of flutter was assessed using a combination of polynomial chaos (PC) expansions and Monte-Carlo simulations. Likewise, Scarth and Cooper [14] used Gaussian process surrogate models to estimate the probability of failure of a composite plate and used reliability-based design to reduce the probability of failure and increase the stability margin. Similar work was also considered by Stanford and Beran [15], but with uncertainty in the panel boundary conditions. Petit and Grandhi [16] performed a reliability-based weight optimization of a wing structure subject to gust response and aileron effectiveness constraints.

Although there have been several studies on the optimization of deterministic aeroservoelastic systems [17], little work has been done on the application of UQ techniques to optimize aeroservoelastic systems with uncertainties.

In this study, UQ and global optimization techniques are coupled to design an active flutter suppression system for a three-degree-of-freedom aeroservoelastic system with parameter uncertainties. In the proposed approach, the mean flutter speed is assigned and the variability is reduced by iteratively updating the gains of a feedback control law. The flutter speed variability is assessed probabilistically by Monte-Carlo simulation of the flutter speed response surface. To reduce the optimization's computational time, the response surface is approximated by a surrogate model, which is constructed using local sensitivities or polynomial chaos expansions.

The remainder of this paper is divided as follows. In Section III a simple deterministic aeroservoelastic system is modelled. This is used as a basis on which to test the proposed method later in the paper. Next, Section IV discusses the effect of uncertainty on the flutter speed. The flutter speed is illustrated as a hypersurface that is a function of the

random parameters and the gains in the control law. It is shown how a surrogate model of the hypersurface can be constructed using either local sensitivities or a polynomial chaos expansion. Section V discusses the optimization framework used to minimize the flutter speed variability. Finally, the method is tested in the form of case studies in Section VI and conclusions are drawn in Section VII.

III. Deterministic Aeroservoelastic System

A. Numerical Modelling

1. Aeroelastic Model

Consider the aeroelastic system shown schematically in Fig. 1. The position is fully described by the vector of degrees-of-freedom $\mathbf{q} = (h \quad \alpha \quad \beta)^{\mathrm{T}}$, where h is the plunge displacement (positive downwards), α is the pitch angle (positive clockwise), and β is the control surface deflection (positive clockwise). Under the assumption that the system is linear, the structural equations of motion are

$$\mathbf{M}_{\mathrm{s}}\ddot{\mathbf{q}} + \mathbf{C}_{\mathrm{s}}\dot{\mathbf{q}} + \mathbf{K}_{\mathrm{s}}\mathbf{q} = \mathbf{f}_{\mathrm{a}} + \mathbf{f}_{\mathrm{c}} \tag{1}$$

where $\mathbf{M}_{\mathrm{s}}, \mathbf{C}_{\mathrm{s}}, \mathbf{K}_{\mathrm{s}} \in \mathbb{R}^{3\times3}$ are the structural mass, damping and stiffness matrices respectively; $\mathbf{f}_{\mathrm{a}} = \begin{pmatrix} -L & M_\alpha & M_\beta \end{pmatrix}^{\mathrm{T}}$ is the aerodynamic force vector; and $\mathbf{f}_{\mathrm{c}} = \begin{pmatrix} 0 & 0 & T_\beta \end{pmatrix}^{\mathrm{T}}$ is the control force vector, which contains the torque used to assign a desired control surface deflection. More detailed expressions for the vectors and matrices described above and hereinafter may be found in Appendix A.

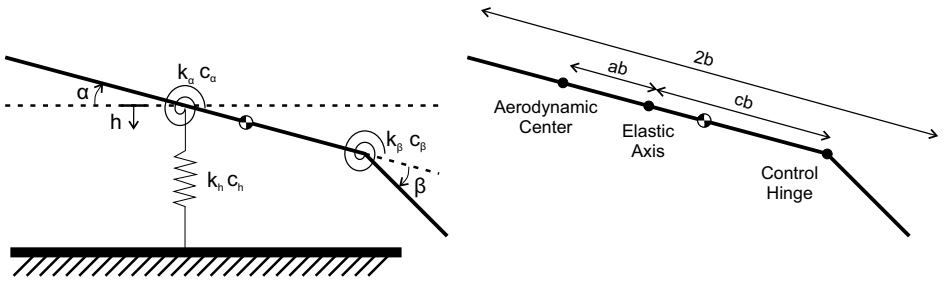

Fig. 1 Pitch-plunge aeroelastic system with a trailing-edge control surface.

In this study, an unsteady, two-dimensional, inviscid aerodynamic model is employed, which is based on the work of Theodorsen [18]. Under this assumption, the aerodynamic force vector is written as

$$\mathbf{f}_a = -\mathbf{M}_{\mathrm{a}}\ddot{\mathbf{q}} - v\mathbf{C}_{\mathrm{a}}\dot{\mathbf{q}} - v^2\mathbf{K}_{\mathrm{a}}\mathbf{q} + \mathbf{f}_{\mathrm{a,circ}}(t) \tag{2}$$

where $\mathbf{M}_{\mathrm{a}}, \mathbf{C}_{\mathrm{a}}, \mathbf{K}_{\mathrm{a}} \in \mathbb{R}^{3\times3}$ are aerodynamic equivalent mass, damping and stiffness matrices respectively; v is the velocity of the freestream; and $\mathbf{f}_{\mathrm{a,circ}}(t) \in \mathbb{R}^3$ is the time-variant aerodynamic force. The rightmost term in Eq. (2) arises from the circulation in the aerodynamics. Using Jones' approximation [19], the circulatory term can be replaced by

$$\mathbf{f}_{a,\mathrm{circ}}(t) = v\mathbf{a}\mathbf{S}_{\mathrm{c}}^T(v)\boldsymbol{\phi} + \frac{1}{2}v^2\mathbf{a}\mathbf{c}_1^T\mathbf{q} + \frac{1}{2}v\mathbf{a}\mathbf{c}_2^T\dot{\mathbf{q}} \tag{3}$$

where $\mathbf{a}, \mathbf{c}_1, \mathbf{c}_2 \in \mathbb{R}^3$; and $\mathbf{S}_{\mathrm{c}}, \boldsymbol{\phi} \in \mathbb{R}^2$. The vector $\boldsymbol{\phi}$ is the aerodynamic state vector, which obeys the evolutionary equation

$$\dot{\boldsymbol{\phi}} = \mathbf{S}_{\mathrm{A}}(v)\boldsymbol{\phi} + v\mathbf{S}_{\mathrm{B}}\mathbf{c}_1^T\mathbf{q} + \mathbf{S}_{\mathrm{B}}\mathbf{c}_2^T\dot{\mathbf{q}} \tag{4}$$

where $\mathbf{S}_A \in \mathbb{R}^{2\times2}$, and $\mathbf{S}_B \in \mathbb{R}^2$. By combining Eqs. (1), (2) and (3), the coupled aeroelastic equations of motion are

$$(\mathbf{M}_{\mathrm{s}} + \mathbf{M}_{\mathrm{a}})\ddot{\mathbf{q}} + \left(\mathbf{C}_{\mathrm{s}} + v\mathbf{C}_{\mathrm{a}} - \frac{1}{2}v\mathbf{a}\mathbf{c}_2^T\right)\dot{\mathbf{q}} + \left(\mathbf{K}_{\mathrm{s}} + v\mathbf{K}_{\mathrm{a}} - \frac{1}{2}v^2\mathbf{a}\mathbf{c}_1^T\right)\mathbf{q} = v\mathbf{a}\mathbf{S}_{\mathrm{c}}\boldsymbol{\phi} + \mathbf{f}_{\mathrm{c}} \tag{5}$$

2. Aeroservoelastic Model

Commonly, the control surface deflection is modelled as an input variable [20] or approximated as a second-order system that has a desired control surface deflection as its input [21]. Whilst these approaches are advantageous in that they do not require an explicit expression for the control torque T_β, they approximate or mitigate the dynamic of the controller itself [22]. In this work, the trailing-edge control surface is actuated by a DC motor that is operated by a proportional-integral-derivative (PID) controller. This is represented in block diagram form in Fig. 2.

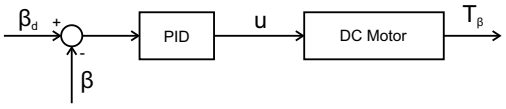

Fig. 2 Block diagram of the inner control loop.

Assuming an ideal motor, a current input yields a proportional torque output and thus

$$T_\beta = k_t u \tag{6}$$

where k_t is the torque constant of the motor, and u is the control current. The current output from the PID is related to the desired and instantaneous control surface deflection by

$$u = k_p\left(\beta_d - \beta\right) + k_d\left(\dot{\beta}_d - \dot{\beta}\right) + k_i \int \left(\beta_d - \beta\right) \mathrm{d}t \tag{7}$$

where k_p, k_i and k_d are the proportional, integral and derivative gains of the PID respectively; and β_d is the desired control surface deflection. Note that, in practice, the output from the PID may be a voltage. In this case, there is a driver between the PID and motor that serves as a gain to transform the voltage to a current.

Suppose that a feedback controller is used so that

$$\beta_d = \mathbf{f}^T\dot{\mathbf{q}} + \mathbf{g}^T\mathbf{q} \tag{8}$$

Using Eqs. (6), (7) and (8), the total control force vector can be written in the form

$$\mathbf{f}_c = -\mathbf{M}_c\ddot{\mathbf{q}} - \mathbf{C}_c\dot{\mathbf{q}} - \mathbf{K}_c\mathbf{q} - \mathbf{N}_c\int \mathbf{q}\mathrm{d}t \tag{9}$$

where $\mathbf{M}_\mathrm{c}, \mathbf{C}_\mathrm{c}, \mathbf{K}_\mathrm{c} \in \mathbb{R}^{3\times3}$ are the control equivalent mass, damping and stiffness matrices respectively; and $\mathbf{N}_c \in \mathbb{R}^{3\times3}$ is the matrix arising from the integral term in the PID.

With expressions for the structural, aerodynamic and control equations derived, it is now possible to write the aeroservoelastic system in autonomous state-space form. Choosing $\mathbf{x} = \begin{pmatrix}\int \mathbf{q}\mathrm{d}t & \mathbf{q} & \dot{\mathbf{q}} & \boldsymbol{\phi}\end{pmatrix}^\mathrm{T}$ as the state vector and using Eqs. (4), (5) and (9), it can be shown that

$$\dot{\mathbf{x}} = \begin{bmatrix} \mathbf{0}_{3\times3} & \mathbf{I}_{3\times3} & \mathbf{0}_{3\times3} & \mathbf{0}_{3\times2} \\ \mathbf{0}_{3\times3} & \mathbf{0}_{3\times3} & \mathbf{I}_{3\times3} & \mathbf{0}_{3\times2} \\ -\mathbf{M}_\mathrm{t}^{-1}\mathbf{N}_c & -\mathbf{M}_\mathrm{t}^{-1}\mathbf{K}_t(v) & -\mathbf{M}_\mathrm{t}^{-1}\mathbf{C}_t(v) & v\mathbf{M}_\mathrm{t}^{-1}\mathbf{a}\mathbf{S}_c \\ \mathbf{0}_{3\times3} & v\mathbf{S}_\mathrm{B}\mathbf{c}_1^T & \mathbf{S}_\mathrm{B}\mathbf{c}_2^T & \mathbf{S}_A(v) \end{bmatrix}\mathbf{x} = \mathbf{A}(v,\mathbf{f},\mathbf{g})\mathbf{x} \tag{10}$$

The coupled structural, aerodynamic and control system is shown in block diagram form in Fig. 3.

B. Deterministic Flutter Condition

The state matrix $\mathbf{A}$ is a function of both the freestream speed and the feedback control gains. As a consequence, its eigenvalues are variable with respect to these quantities, i.e. $\lambda = \lambda(v,\mathbf{f},\mathbf{g})$. By definition, the flutter speed is the freestream speed at which the system becomes unstable. By defining the function

$$G(\lambda(v,\mathbf{f},\mathbf{g})) = \max_i(\mathrm{Re}(\lambda_i(v,\mathbf{f},\mathbf{g}))) \tag{11}$$

where λ_i is the i^{th} eigenvalue of the state matrix $\mathbf{A}$, the flutter condition is

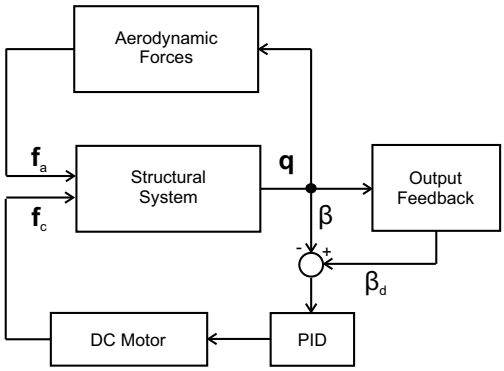

Fig. 3 Coupled structural, aerodynamic and control systems.

$$G(\lambda(v_f, \mathbf{f}, \mathbf{g})) = 0 \tag{12}$$

where v_f is the flutter speed. The physical interpretation of Eq. (12) is that the system is marginally stable when one of the eigenvalues lies on the imaginary axis in the complex plane.

IV. Uncertain Flutter Boundary

A. Flutter Speed Variability

Suppose that the system described in Section III-A has uncertainty in p parameters. The state matrix of Eq. (10) becomes a function of p random variables and thus the uncertain aeroservoelastic system is governed by

$$\dot{\mathbf{x}} = \mathbf{A}(v, \{\zeta_i\}_{i=1}^{p}, \mathbf{f}, \mathbf{g})\mathbf{x} \tag{13}$$

where ζ_i is the set of uncertain parameters. Using the same procedure of Section III-B, the new flutter condition is

$$G(\lambda(v_f, \{\zeta_i\}_{i=1}^{p}, \mathbf{f}, \mathbf{g})) = 0 \tag{14}$$

and hence the flutter speed becomes a random variable.

When the control gains **f** and **g** are fixed, the flutter speed becomes a function of only the random parameters. In this case, the flutter speed is visualized as a p dimensional hypersurface. A typical example of this is shown in Fig. 4(a) for the case of two parameters. The mean flutter speed corresponds to the point shown in red and the height difference between this point and all other points in the surface corresponds to the flutter speed variability. When the control gains

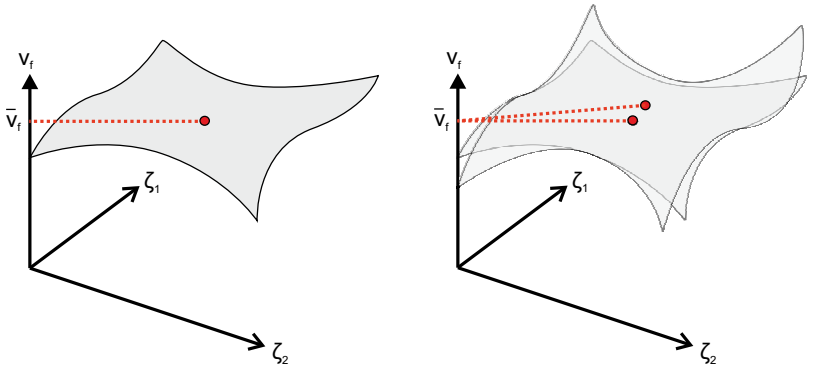

(a) Initial control gains. (b) Modified control gains.

Fig. 4 Flutter surface for two random parameters.

are changed, the shape of the surface is modified. Fig. 4(b) shows an example of this effect, again for the case of two parameters. Most notably, the curvature is altered and therefore so too is the variability of the flutter speed.

In some cases, it is possible to modify the control gains so that the mean flutter speed remains constant. This means that there exists multiple sets of control gains that achieve the same mean flutter speed but with different levels of variability with respect to the random parameters. It is hypothesized, therefore, that optimal control gains that minimize the variability of the flutter speed can be selected even though the mean flutter speed remains constant.

In order to evaluate the variability of the flutter speed probabilistically, Monte Carlo simulation (MCS) is used. Performing MCS on Eq. (14) directly is computationally expensive given the need to compute eigenvalues of the state matrix and iteratively update the freestream speed to find the flutter speed. Instead, it is more efficient to sample a surrogate model.

B. Approximation of the Flutter Boundary using Local Sensitivities

The simplest way in which to form a surrogate model of the flutter hypersurface is to linearize it about the mean random parameters. In this way,

$$v_f \approx v_n + \sum_{i=1}^{p} \frac{\partial v_f}{\partial \zeta_i}(\zeta_i - \bar{\zeta}_i) \tag{15}$$

As shown by Beran and Stanford [9], the partial derivatives in Eq. (15) are related to the state matrix by

$$\frac{\partial v_f}{\partial \zeta_i} = -\mathrm{Re}\left[\left(\boldsymbol{\phi}_\mathrm{L}^\dagger \frac{\partial \mathbf{A}}{\partial \zeta_i}\boldsymbol{\phi}_\mathrm{R}\right) / \left(\boldsymbol{\phi}_\mathrm{L}^\dagger \boldsymbol{\phi}_\mathrm{R}\right)\right] / \mathrm{Re}\left[\left(\boldsymbol{\phi}_\mathrm{L}^\dagger \frac{\partial \mathbf{A}}{\partial v}\boldsymbol{\phi}_\mathrm{R}\right) / \left(\boldsymbol{\phi}_\mathrm{L}^\dagger \boldsymbol{\phi}_\mathrm{R}\right)\right] \tag{16}$$

where $\boldsymbol{\phi}_\mathrm{L}$, $\boldsymbol{\phi}_\mathrm{R}$ are the left and right eigenvectors of the state matrix corresponding to the unstable eigenvalue at flutter, and $\dagger$ denotes the Hermitian transpose operator. When the surface is linearized, the mean flutter speed corresponds to the surface height at the mean parameter values, i.e.

$$v_n = \bar{v}_f \tag{17}$$

The advantages of using local sensitivities to represent the flutter boundary are that: 1) analytical expressions for the sensitivities are available and thus are simple to compute, and 2) the simplicity of the resulting surface permits efficient sampling to obtain probabilistic information of the flutter speed quickly. The problem, however, is that the linear approximation works well only when the second and higher-order derivatives of the true flutter surface are small across the region of interest. Extrapolating the linear approximation far from the average flutter speed may result in a large degree of error between the true and estimated flutter speed.

C. Approximation of the Flutter Boundary using a Polynomial Chaos Expansion

To overcome the limitations of linearizing the flutter boundary, a higher-order approximation may be used. One approach is to use a polynomial chaos (PC) expansion, which expresses the flutter speed as the sum of weighted functions that are orthogonal to each other. Written mathematically,

$$v_f = \sum_{i=0}^{\infty} a_i \Psi_i\left(\{\zeta_i\}_{i=1}^{p}\right) \tag{18}$$

where a_i are weighting constants and Ψ_i are the multidimensional orthogonal functions. When the parameters ζ_i follow a standard normal distribution, the orthogonal functions are the multidimensional Hermite polynomials [23]. For computational implementation, the expansion is truncated to the first N terms and thus

$$v_f \approx \sum_{i=0}^{N} a_i \Psi_i\left(\{\zeta_i\}_{i=1}^{p}\right) \tag{19}$$

As Eldred [24] explains, there are two distinct ways to extract the coefficients of the expansion; intrusive and non-intrusive methods. In this work, a non-intrusive method is used, where the true flutter surface is sampled and the coefficients in the surrogate are found by least squares estimation. The mean flutter speed may be evaluated simply from the first coefficient of the expansion,

$$\bar{v}_f = a_0 \tag{20}$$

The significant advantage of using PC expansions over local sensitivities is that the approximated flutter boundary is not limited to first-order. In theory, the error between the approximated and actual flutter boundary should be less as it is able to capture nonlinear behavior. The problem with this approach, however, is that sampling from the true flutter boundary is required to obtain the expansion coefficients and thus the computational time is increased.

V. Control Optimization

In deterministic aeroservoelastic systems, the control gains are selected so that the flutter speed is increased subject to the limits of the controller. However, when uncertainties are present, the controller must increase the flutter speed at minimal cost to its variability. Here, a global optimization approach is used to solve this problem, which is cast as

$$\begin{aligned} \underset{\mathbf{f},\mathbf{g}}{\text{minimize}} \quad & f_{\text{variability}}(\mathbf{f},\mathbf{g}) \\ \text{subject to} \quad & \bar{v}_f = v_{f,\text{desired}} \\ & g_i(\mathbf{f},\mathbf{g}) \quad i = 1, 2, ..., n \end{aligned} \tag{21}$$

where $f_{\text{variability}}$ is a function that evaluates the variability of the flutter speed, $v_{f,\text{desired}}$ is the desired mean flutter speed, and g_i are controller constraints. Typically, the controller constraints are based on the maximum deflection angle of the control surface and the maximum control torque.

In the probabilistic approach, the variability function is defined as

$$f_{\text{variability}}(\mathbf{f},\mathbf{g}) = F^{-1}(p), \quad p \in [0,1] \tag{22}$$

where F^{-1} is the inverse cumulative distribution function of the flutter speed and p is the worst-case probability, which is chosen.

An overview of the proposed method is shown in Fig 5.

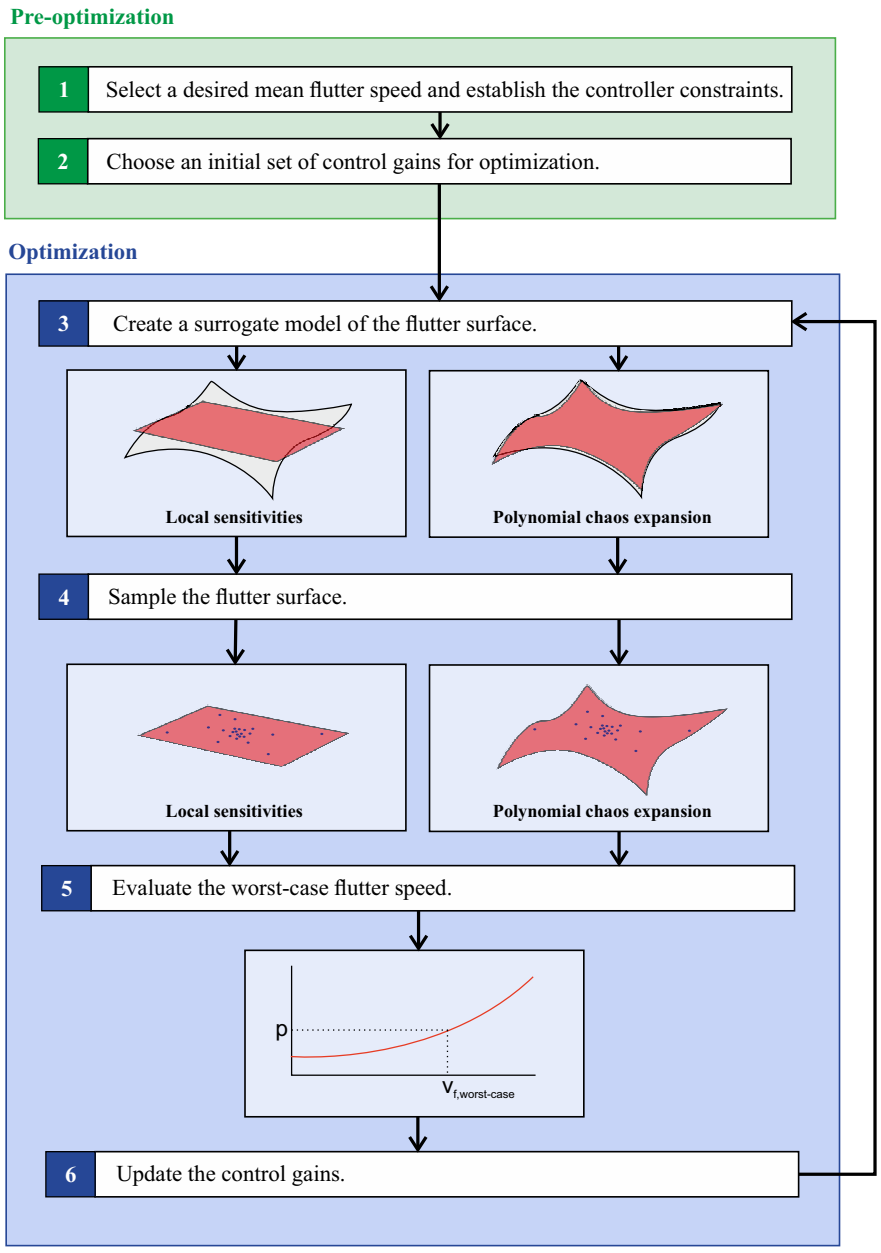

Fig. 5 Method overview.

VI. Numerical Example

Here, the proposed method is tested numerically on a three-degree-of-freedom aeroservoelastic system with nominal parameters as given in Appendix B. The pitch and plunge stiffness values are the uncertain parameters and are assumed normally distributed with a coefficient of variation of 5%.

A. Inactive Controller

When the high-level controller is inactive, i.e. $\mathbf{f} = \mathbf{g} = \mathbf{0}$, the control surface deflection is held at zero degrees and is independent of the position and velocity of the pitch and plunge degrees-of-freedom. In this case, the mean flutter speed is 15.01 m/s. The variability of the flutter speed, which arises from the uncertain stiffness values, is shown diagrammatically in Fig. 6. The terms z_1 and z_2 correspond to the normalized plunge and pitch stiffness parameters respectively, i.e.

$$z_1 = \frac{k_h - \mathrm{E}[k_h]}{\sqrt{\mathrm{Var}[k_h]}}, \quad z_2 = \frac{k_\alpha - \mathrm{E}[k_\alpha]}{\sqrt{\mathrm{Var}[k_\alpha]}}$$

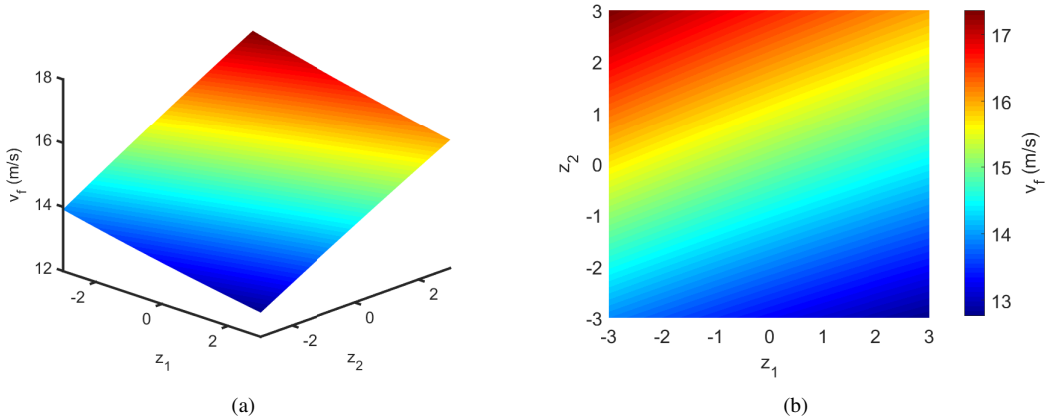

Fig. 6 Flutter speed variability with zero gains.

When a surrogate model of the flutter surface is created using local sensitivities, as in Eq. (15), the percentage error between the true and approximated surface is low, as shown in Fig. 7(a). This is because the true flutter surface is closely linear and therefore the approximation serves well. Likewise, a third-order PC expansion surrogate model, constructed by 40 Latin Hypercube samples, yields very little discrepancy between the true and estimated flutter speeds, as illustrated in Fig. 7(b). As expected, the PC expansion errors are lower across the ranges investigated as it is able to capture the slight nonlinear behavior in the flutter surface.

Figure 8 shows a comparison of the flutter speed cumulative distribution function (CDF) found from Monte-Carlo simulation of Eq. (14) directly and by sampling of the two surrogate models. In all three cases, 100,000 samples are used. The discrepancy between the three distributions is very low. Indeed, the flutter speed corresponding to the 1% worst-case varies only by 0.01 m/s.

B. Active Controller

Now, the high-level controller is switched on and the gains are selected such that: 1) the mean flutter speed is increased to 18.0 m/s, 2) the maximum control surface deflection is less than 10 degrees, and 3) the required motor torque is no greater than 15.4 mN m. The maximum torque is selected based on a typical value for a control surface of the size considered in these examples. Three cases are presented that demonstrate how the choice of control gains significantly affects the variability of the flutter speed.

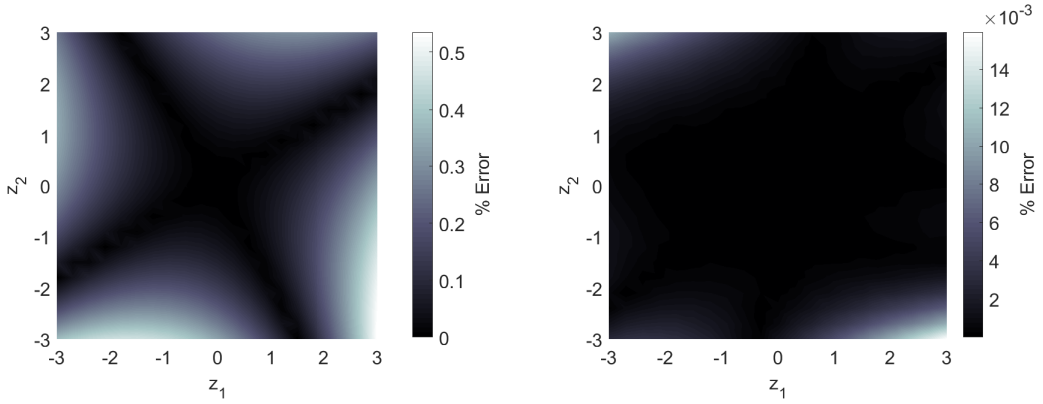

(a) Local sensitivities. (b) PC expansion.

Fig. 7 Percentage error between the true and approximated flutter surface.

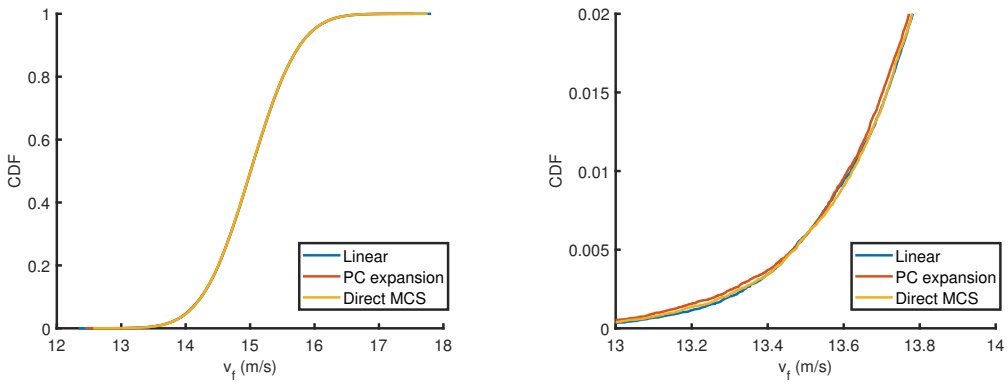

(a) (b) CDF at the worst-case speed.

Fig. 8 Flutter speed CDF with zero control gains.

1. Case 1: Sub-optimal Choice of Control Gains

Suppose that the control gains $\mathbf{f} = [0.0265, -0.1, 0]^T$ and $\mathbf{g} = [-4, -1.5, 0]^T$ are selected, without consideration of the flutter speed variability, so that the constraints are satisfied. Note that the third term in each gain vector is zero since only feedback from the pitch and plunge is used. With the control gains applied, Fig. 9 shows the new, modified flutter surface. As required by the constraints, the mean flutter speed is now 18 m/s. However, the variability of the flutter speed has also changed.

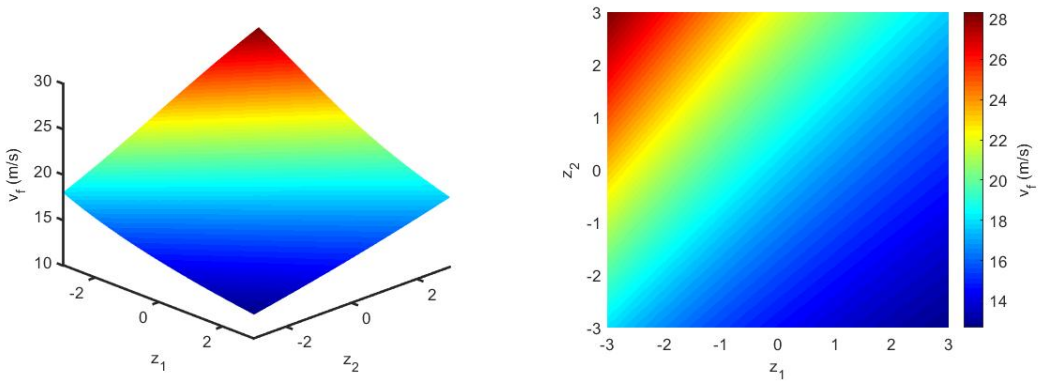

(a) (b)

Fig. 9 Flutter speed variability (case 1).

Due to the larger curvature of the true flutter surface, it is anticipated that the approximation using local sensitivities will only work in the region close to the expected flutter speed. This is confirmed by Fig. 10(a), which shows the percentage error between the true and estimated flutter speed. Crucially, the lower flutter speeds have a maximum percentage error of approximately 18%. This means that estimation of the probabilistic worst-case flutter speed will likely be inaccurate. When a PC expansion is used to approximate the flutter surface, the maximum error is reduced by approximately 75%, as shown in Fig. 10(b). Moreover, the largest error corresponds to the point where the flutter velocity is highest and therefore it is unlikely that this will affect the calculation of the worst-case flutter speed.

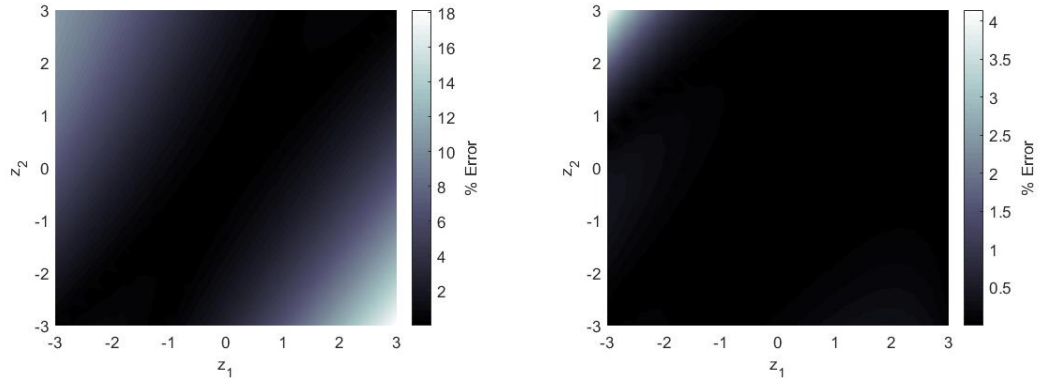

(a) Local sensitivities (b) PC expansion

Fig. 10 Percentage error between the true and approximated flutter surface (case 1).

Figure 11 shows a comparison of the CDF of the flutter speed by direct MCS and by sampling of the two surrogate models. Close to the mean flutter speed, the distributions vary little. However, at the extreme values, there is a discrepancy between the distributions. At a 1% worst-case flutter speed, the difference is approximately 0.9 m/s (6 %). Given the closeness of the PC expansion and direct MCS results, the 1% worst-case speed is taken as 14.6 m/s.

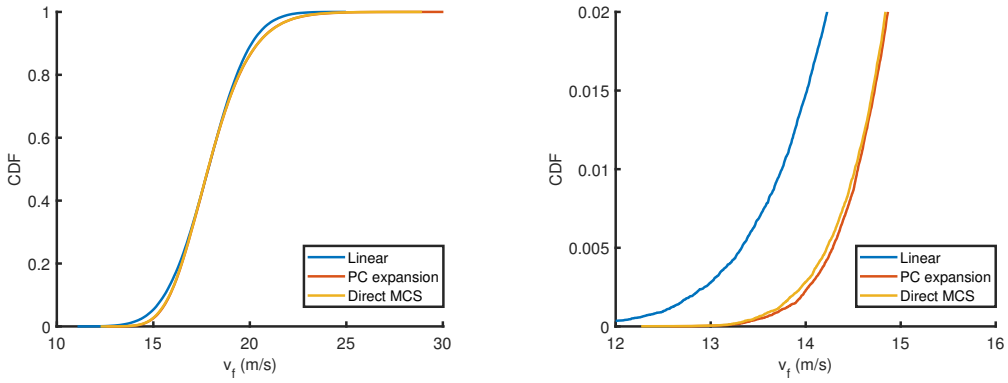

(a) (b) CDF at the worst-case speed.

Fig. 11 Flutter speed CDF (case 1).

This case highlights the limitations of using local sensitivities to estimate the flutter surface and its corresponding worst-case flutter speed. In general, there is no guarantee that the flutter surface is closely linear and therefore PC expansions produces a more accurate representation of the flutter surface compared with local sensitivities.

Although local sensitivities can lead to poor estimates of the worst-case flutter speed, they may still give a loose indication to the flutter speed variability and therefore could be used in an optimization framework. This will be tested in the following case.

2. Case 2: Optimization using Local Sensitivities

Here, the optimization framework described in Sec. V is used to optimally select the control gains such that the worst-case flutter speed is as large as possible. The flutter surface is approximated using local sensitivities and the Differential Evolution algorithm by Storn and Price [25] is used to perform global optimization subject to the aforementioned constraints. The optimal control gains are found to be $\mathbf{f} = [0.2701, -0.1, 0]^T$ and $\mathbf{g} = [-2.571, -0.643, 0]^T$. The variability of the flutter speed is shown in Fig. 12 and the 1% worst-case flutter speed is computed as 15.4 m/s. By comparison with the results of case 1, the worst-case speed is higher and thus the variability of the flutter speed about its mean (18.0 m/s) is lower, as was required.

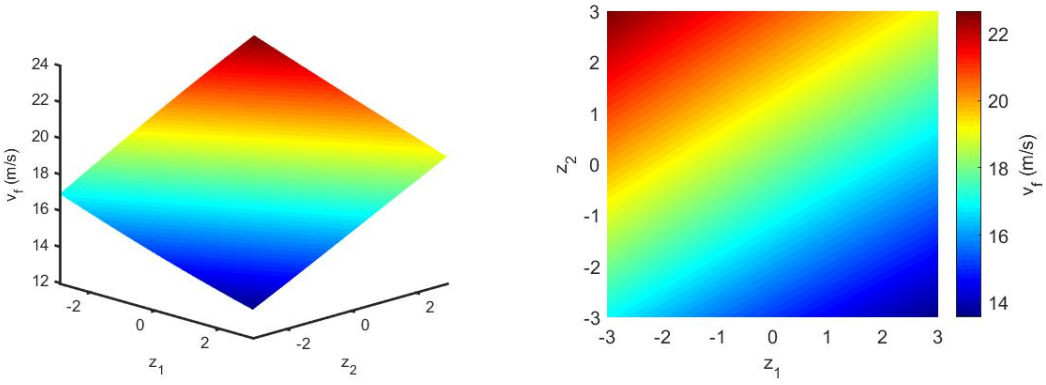

(a) (b)

Fig. 12 Flutter speed variability (case 2).

The error between the true and estimated flutter speeds is shown in Fig. 13. In this case, the linear approximation of the flutter surface works well. It should be noted, however, that there is no guarantee that the linear approximation works

well during the optimization process. As has already been shown, the control gains significantly affect the degree of nonlinearity in the flutter surface and therefore there may be iterations where the linear approximation yields erroneous worst-case flutter speeds. As a result, there is no assurance that the sensitivities-based optimization produces the best solution possible.

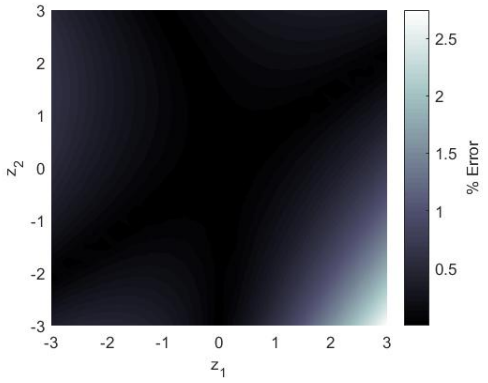

Fig. 13 Percentage error between the true and approximated flutter surface (case 2).

3. Case 3: Optimization using a PC expansion

Finally, the optimization is performed again but using a PC expansion as a surrogate of the flutter surface. Using the same optimization settings as before, the new optimal control gains are $\mathbf{f} = [-0.1805, 0.0058, 0]^T$ and $\mathbf{g} = [1.28, -1.286, 0]^T$. The resulting flutter surface for these new gains is shown in Fig. 14.

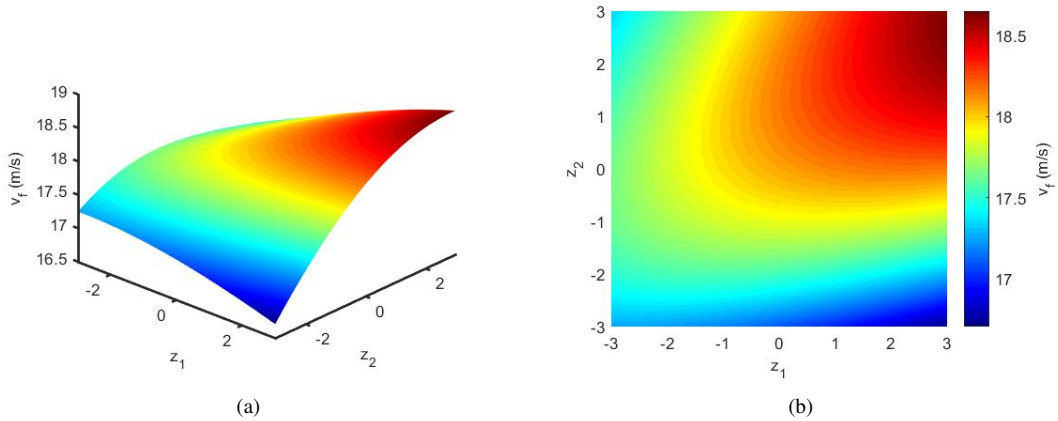

Fig. 14 Flutter speed variability (case 3).

The new flutter surface is considerably different to that of case 2. Firstly, the variability of the flutter speed is significantly less. The new 1% worst-case flutter speed is 17.4 m/s. In addition, the shape of the surface is now highly nonlinear. This suggests that the PC expansion optimization is able to exploit nonlinearities in the flutter surface, which local sensitivities are unable to do. The error between the true and estimated flutter speed is shown in Fig. 15. In this case, the approximation serves well.

4. Comparison

A comparison of the results from the above three cases are given in Table 1 and the corresponding CDFs are shown in Fig. 16. As shown, it is possible to assign a mean flutter speed using different sets of feedback control gains.

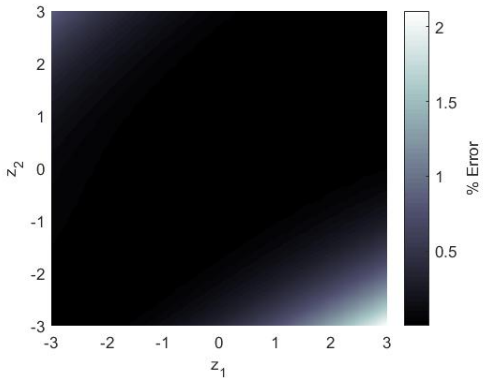

Fig. 15 Percentage error between the true and approximated flutter surface (case 3).

However, these values significantly influence the variability of the flutter speed. Indeed, the worst-case flutter speed can be increased from 14.7 m/s to 17.4 m/s (18%) by means of optimization.

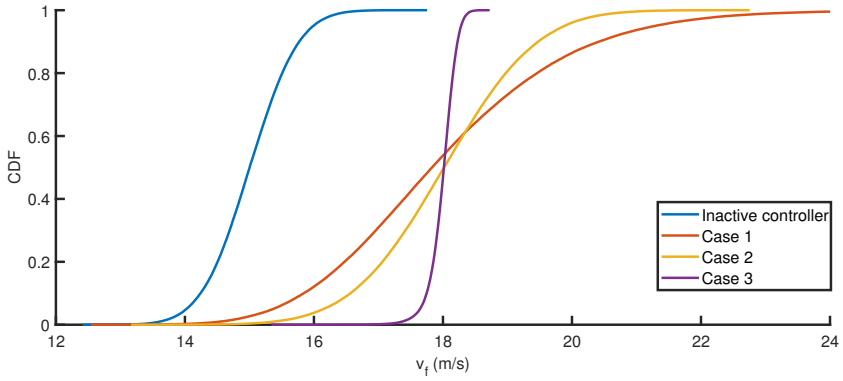

Fig. 16 Comparison of flutter speed CDF with different control gains,

Table 1 Worst-case flutter speed for each optimization case.

Case	Worst-case flutter speed (m/s)
1	14.7
2	15.4
3	17.4

Figure 17 shows the variability of the pitch and plunge poles with the freestream velocity as the different control gains are applied. The bounds correspond to the extremities between ±2.5 standard deviations of the random parameters. Note that the pole corresponding to the controller is at a much higher frequency and therefore is not shown. In the inactive controller case, case 1, and case 2, the parameter variability keeps the overall shape of the pole paths relatively unchanged. In case 3, the shape changes considerably and suggests, as mentioned previously, that the control gains are exploiting a nonlinearity in the flutter speed response surface.

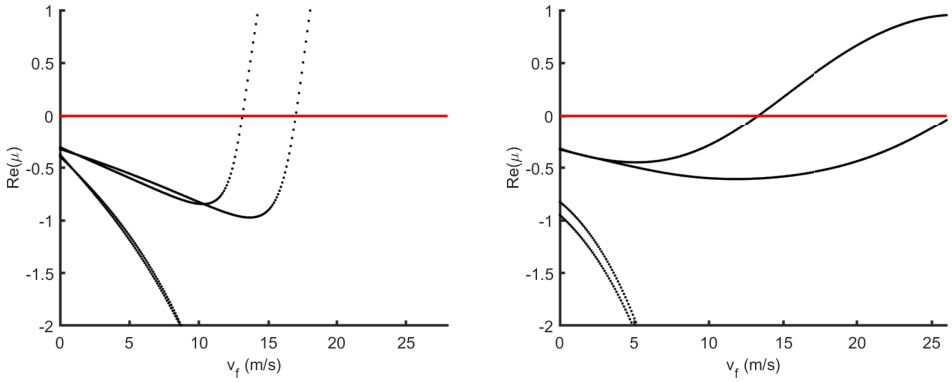

(a) Inactive controller.

(b) Case 1.

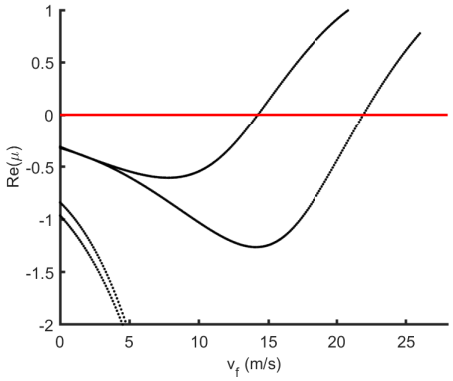

(c) Case 2.

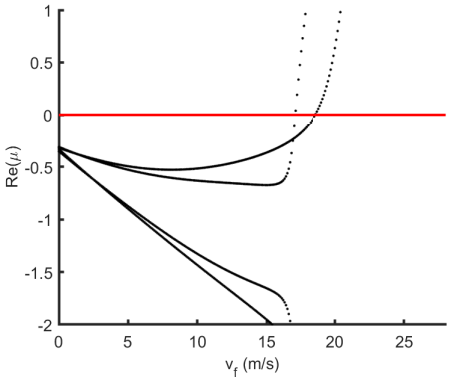

(d) Case 3.

Fig. 17 Unstable pole paths with different control gains between ±2.5 standard deviations of the random parameters.

VII. Conclusions

A global optimization technique for aeroservoelastic systems with parameter uncertainty has been developed. The mean flutter speed was assigned by means of feedback control acting through a trailing-edge control surface. It was shown that different combinations of control gains achieved the same mean speed but with various levels of flutter speed variability. As a result, it was hypothesized that an optimization approach could be used to find the optimum set of control gains that both assigned a mean speed and minimized its variability. In the proposed method, the variability was assessed probabilistically by first sampling the uncertain flutter hypersurface and then by constructing the inverse cumulative density function of the flutter speed. The worst-case flutter speed was then extracted based on the probability that the flutter speed was less than or equal to a chosen value. For reasons of computational efficiency, a surrogate model of the hypersurface was constructed using either local sensitivities or a polynomial chaos expansion. Although the local sensitivities approximation successfully increased the worst-case flutter speed, it did not achieve as good of a solution as that with a polynomial chaos expansion approximation. This is because the local sensitives were unable to capture nonlinear behavior in the hypersurface and consequently led to large errors between the true and estimated flutter speed.

Appendices

A. Detailed Matrix and Vector Expressions

1. Structural Matrices

$$\mathbf{M}_s = \begin{bmatrix} M & S_\alpha & S_\beta \\ S_\alpha & I_\alpha & I_\beta + b(c-a)S_\beta \\ S_\beta & I_\beta + b(c-a)S_\beta & I_\beta \end{bmatrix}, \quad \mathbf{C}_s = \begin{bmatrix} c_h & 0 & 0 \\ 0 & c_\alpha & 0 \\ 0 & 0 & c_\beta \end{bmatrix}, \quad \mathbf{K}_s = \begin{bmatrix} k_h & 0 & 0 \\ 0 & k_\alpha & 0 \\ 0 & 0 & k_\beta \end{bmatrix}$$

2. Aerodynamic Matrices

$$\mathbf{M}_a = \rho s_T \begin{bmatrix} \pi b^2 & -\pi b^3 a & -b^3 T_1 s_C \\ -\pi b^3 a & \pi b^4(\frac{1}{8} + a^2) & -b^4(T_7 + (c-a)T_1)s_C \\ -b^3 T_1 s_C & 2b^4 T_{13} s_C & -\frac{b^4}{\pi} T_3 s_C \end{bmatrix},$$

$$\mathbf{C}_a = \rho s_T \begin{bmatrix} 0 & \pi b^2 & -b^2 T_4 s_C \\ 0 & \pi b^3(\frac{1}{2} - a) & -b^3(T_8 - T_1 + (c-a)T_4 - \frac{T_{11}}{2})s_C \\ 0 & -b^3(2T_9 + T_1 + (\frac{1}{2} - a)T_4)s_C & -\frac{b^3}{2\pi} T_{11} T_4 s_C \end{bmatrix},$$

$$\mathbf{K}_a = \rho s_T \begin{bmatrix} 0 & 0 & 0 \\ 0 & 0 & b^2(T_4 + T_{10})s_C \\ 0 & 0 & \frac{b^2}{\pi}(T_5 - T_4 T_{10})s_C \end{bmatrix},$$

$$\mathbf{a} = \rho s_T \begin{bmatrix} -2\pi b \\ 2\pi b^2(\frac{1}{2} + a) \\ -b^2 T_{12} s_C \end{bmatrix}, \quad \mathbf{c}_1 = \begin{bmatrix} 0 \\ 1 \\ \frac{T_{10}}{\pi} \end{bmatrix}, \quad \mathbf{c}_2 = \begin{bmatrix} 1 \\ b(\frac{1}{2} - a) \\ \frac{b}{2\pi} T_{11} \end{bmatrix}$$

$$\mathbf{S}_A = \begin{bmatrix} -0.3455\left(\frac{v}{b}\right) & -0.01365\left(\frac{v}{b}\right)^2 \\ 1 & 0 \end{bmatrix}, \quad \mathbf{S}_B = \begin{bmatrix} 1 \\ 0 \end{bmatrix}, \quad \mathbf{S}_C^T = \begin{bmatrix} 0.1082\left(\frac{v}{b}\right) & 0.006825\left(\frac{v}{b}\right)^2 \end{bmatrix},$$

The terms T_x are the Theodorsen coefficients described in [18].

3. Control Matrices

$$\mathbf{M}_c = -k_m k_d \mathbf{e}\mathbf{f}^T$$

$$\mathbf{C}_c = -k_m k_p \mathbf{e}\mathbf{f}^T - k_m k_d \mathbf{e}\left(\mathbf{g}^T - \mathbf{e}^T\right)$$

$$\mathbf{K}_c = -k_m k_i \mathbf{e}\mathbf{f}^T - k_m k_p \mathbf{e}\left(\mathbf{g}^T - \mathbf{e}^T\right)$$

$$\mathbf{N}_c = -k_m k_i \mathbf{e}\left(\mathbf{g}^T - \mathbf{e}^T\right)$$

$$\mathbf{e}^T = \begin{bmatrix} 1 & 0 & 0 \end{bmatrix} \tag{23}$$

4. Total Matrices

$$\mathbf{M}_t = \mathbf{M}_s + \mathbf{M}_a + \mathbf{M}_c, \quad \mathbf{C}_t = \mathbf{C}_s + \mathbf{C}_a + \mathbf{C}_c - \frac{1}{2}\mathbf{a}\mathbf{c}_2^T, \quad \mathbf{K}_t = \mathbf{K}_s + \mathbf{K}_a + \mathbf{K}_c - \frac{1}{2}\mathbf{a}\mathbf{c}_1^T$$

B. Nominal Parameters

Table 2 Nominal parameters for the aeroservoelastic system

Parameter	Value	Unit
M	11.142	kg
I_α	0.0278	kg m^2
I_β	5.65×10^{-5}	kg m^2
S_α	0.158	kg m
S_β	1.42×10^{-3}	kg m
k_h	3510	N m^{-1}
k_α	27.347	N rad^{-1}
k_β	0	N rad^{-1}
c_h	7.66	N s m^{-1}
c_α	0.017	N s rad^{-1}
c_β	0	N s rad^{-1}
ρ	1.225	kg m^{-3}
b	0.15	m
a	-0.32	–
c	0.6	–
s_T	1.2	m
s_C	0.25	–
k_t	0.273	mN m A^{-1}
k_p	5	–
k_i	0	–
k_d	0.01	–

Acknowledgments

The authors wish to acknowledge the support provided by the EPSRC Doctoral Training Scholarship.

References

[1] Livne, E., "Aircraft Active Flutter Suppression: State of the Art and Technology Maturation Needs," *Journal of Aircraft*, Vol. 55, No. 1, 2018, pp. 410–452.

[2] Clark, R., and Cox, D., "Aeroelastic Control," *A Modern Course in Aeroelasticity*, edited by E. H. Dowell, Kluwer Academic Publishers, Dordrecht, 2004, 4th ed., pp. 611–674.

[3] Moulin, B., "Modeling of Aeroservoelastic Systems with Structural and Aerodynamic Variations," *AIAA Journal*, Vol. 43, No. 12, 2005, pp. 2503–2513.

[4] Borglund, D., "Robust Eigenvalue Analysis Using the Structured Singular Value: The μ-p Flutter Method," *AIAA Journal*, Vol. 46, No. 11, 2008, pp. 2806–2813.

[5] Lind, R., and Brenner, M., *Robust Aeroservoelastic Stability Analysis*, 1st ed., Springer-Verlag, London, 1999.

[6] Yuting, D., and Chao, Y., "Methods and advances in the study of aeroelasticity with uncertainties," *Chinese Journal of Aeronautics*, Vol. 27, No. 3, 2014, pp. 461–474.

[7] Danowsky, B. P., Chrstos, J. R., Klyde, D. H., Farhat, C., and Brenner, M., "Evaluation of Aeroelastic Uncertainty Analysis Methods," *Journal of Aircraft*, Vol. 47, No. 4, 2010, pp. 1266–1273.

[8] Zhou, K., and Doyle, J. C., *Essentials of Robust Control*, 1st ed., Prentice-Hall, Upper Saddle River, NJ, 1998.

[9] Beran, P., and Stanford, B., "Uncertainty Quantification in Aeroelasticity," *Uncertainty Quantification in Computational Fluid Dynamics*, edited by H. Bijl, D. Lucor, S. Mishra, and C. Schwab, Springer, Cham, 2013, 1st ed., pp. 59–104.

[10] Beran, P., Stanford, B., and Schrock, C., "Uncertainty Quantification in Aeroelasticity," *Annual Review of Fluid Mechanics*, Vol. 49, 2017, pp. 361–386.

[11] Petit, C., "Uncertainty Quantification in Aeroelasticity: Recent Results and Research Challenges," *Journal of Aircraft*, Vol. 41, No. 5, 2004, pp. 1217–1229.

[12] Allen, M., and Maute, K., "Reliability-based design optimization of aeroelastic structures," *Structural and Multidisciplinary Optimization*, Vol. 27, No. 4, 2004, pp. 228–242.

[13] Manan, A., and Cooper, J., "Design of Composite Wings Including Uncertainty: A Probabilistic Approach," *Journal of Aircraft*, Vol. 46, No. 2, 2009, pp. 601–607.

[14] Scarth, C., and Cooper, J. E., "Reliability-based aeroelastic design of composite plate wings using a stability margin," *Structural and Multidisciplinary Optimization*, Vol. 57, No. 4, 2018, pp. 1695–1709.

[15] Stanford, B., and Beran, P., "Minimum-mass panels under probabilistic aeroelastic flutter constraints," *Finite Elements in Analysis and Design*, Vol. 70-71, 2013, pp. 15–26.

[16] Pettit, C. L., and Grandhi, R. V., "Optimization of a Wing Structure for Gust Response and Aileron Effectiveness," *Journal of Aircraft*, Vol. 40, No. 6, 2003, pp. 1185–1191.

[17] Livne, E., "Integrated Aeroservoelastic Optimization: Status and Direction," *Journal of Aircraft*, Vol. 36, No. 1, 1999, pp. 122–145.

[18] Theodorsen, T., "General theory of aerodynamic instability and the mechanism of flutter," Tech. Rep. 495, NACA, 1934.

[19] Jones, R. T., "Operational treatment of the non-uniform lift theory in airplane dynamics," Tech. Rep. 667, NACA, 1938.

[20] Isnardi, I., Paoletti, P., Fichera, S., Miranda, D., and Innocenti, G., "Nonlinear Aeroservoelastic Control Design and Validation," *AIAA Guidance, Navigation, and Control Conference*, Vol. 1, AIAA, Orlando, 2018.

[21] Suzuki, S., and Yonezawa, S., "Simultaenous Structure/Control Design Optimization of a Wing Structure with a Gust Load Alleviation System," *Journal of Aircraft*, Vol. 30, No. 2, 1993, pp. 268–274.

[22] Tewari, A., *Aeroservoelasticity: Modelling and Control*, 1st ed., Springer, New York, 2015.

[23] Ghanem, R. G., and Spanos, P. D., *Stochastic Finite Elements: A Spectral Approach*, 1st ed., Springer-Verlag, New York, 1991.

[24] Eldred, M. S., "Recent Advances in Non-Intrusive Polynomial Chaos and Stochastic Collocation Methods for Uncertainty Analysis and Design," *AIAA/ASME/ASCE/AHS/ASC Structures, Structural Dynamics, and Materials Conference*, AIAA, Palm Springs, 2009.

[25] Storn, R., and Price, K., "Differential Evolution - A Simple and Efficient Heuristic for Global Optimization over Continuous Spaces," *Journal of Global Optimization*, Vol. 11, No. 4, 1997, pp. 341–359.